Computation of wave dispersion characteristics in periodic porous materials modeled as equivalent fluids

D Magliacano, M. Ouisse, A. Khelif, S de Rosa, F Franco, Noureddine Atalla

Computation of wave dispersion characteristics in periodic porous materials modeled as equivalent fluids

D. Magliacano[1,2], M. Ouisse[1], A. Khelif[1], S. De Rosa[2], F. Franco[2], N. Atalla[3]

[1]Univ. Bourgogne Franche-Comté // FEMTO-ST Institute // CNRS/UFC/ENSMM/UTBM
Department of Applied Mechanics // 25000 Besançon, FRANCE

[2]Università degli Studi di Napoli "Federico II" (UniNa)
Corso Umberto I 40, 80138 Napoli, ITALY

[3]Université de Sherbrooke (UdeS)
2500 boul. de l'Université, Sherbrooke (Québec) J1K 2R1, CANADA

e-mail: **dario.magliacano@univ-fcomte.fr**

Abstract

This paper starts with the presentation of the shift cell technique, which allows the description of the propagation of all existing waves starting from the unit cell through a quadratic eigenvalue problem. Its major advantage is that it allows the implementation of any frequency dependence and damping in the problem: this is a fundamental advantage when computing the dispersion curves of a porous material modeled as an equivalent fluid. The second part of this work concerns the investigation of the link between the dispersion curves and the acoustic properties of the material. Deriving the equivalent acoustic properties of the unit cell from its dispersion characteristics, indeed, could be a very efficient approach for designing the sound packages with a simple a preliminary eigenvalue analysis.

List of symbols

- $\omega =$ angular frequency;
- $x, y, z =$ space variables;
- $j =$ imaginary unit;
- $p_0 =$ amplitude of the excitation mode (incident pressure);
- $\rho_0 =$ density of the interstitial fluid (air);
- $c_0 =$ sound speed in the interstitial fluid (air);
- $Z_0 =$ characteristic impedance of the interstitial fluid (air);
- $k_0 =$ wave number in the interstitial fluid (air);
- $\rho =$ density of the material;
- $Z_c =$ characteristic impedance of the material;
- $k =$ wave number in the material;
- $p =$ pressure;
- $K =$ bulk modulus;
- $\theta, \phi =$ angles of incidence;
- $p^* = conj(p)$;
- $\Omega =$ poro-elastic volume;
- $\Gamma =$ domain boundary;
- $I =$ flow of energy;

- $E =$ total energy;
- $E_k =$ kinetic energy;
- $E_p =$ potential energy;
- $v =$ istantaneous local velocity;
- $v_E =$ energy transport speed;
- $C_g =$ group velocity;
- $s =$ side length;
- $\Pi_{incident} =$ incident power;
- $\Pi_{transmitted} =$ transmitted power;
- $S =$ surface interested by incident pressure;
- $d =$ thickness;
- $\tau_\infty =$ transmission coefficient;
- $TL =$ transmission loss.

1 Introduction

The design based on the inclusion of vibroacoustic design rules at early stage of products development, through the use of porous media with periodic inclusions which exhibit proper dynamic filtering effects, is a powerful strategy for the achievement of lightweight sound packages and represents a convenient solution for manufacturing aspects.

The main advantage of designing sound packages with periodic arrangements is that they can provide a combination of absorption effects, resonance effects and wave interferences effects. This offers different applications in transportation (aeronautics, space, automotive, railway), energy and civil engineering sectors, where both weight and space, as well as vibroacoustic integrity and comfort, still remain as critical issues.

Indeed, although porous materials are commonly used for vibroacoustic applications, they suffer from a lack of absorption at low frequencies compared to their efficiency at higher ones. This difficulty is usually overcome by multi-layering. However, while reducing the impedance mismatch at the air-material interface, the efficiency of such devices relies on the allowable thickness. Instead, a more efficient way to enhance the low frequency performances of sound packages consists in embedding periodic inclusions in a porous layer. If the radius of these periodic inclusions is comparable with the acoustic wavelength, then an increase of the acoustical performances can be observed.

In order to develop efficient numerical techniques to handle the problem, the shift cell operator technique here is presented, providing details on its implementation [1]. Essentially, the shift cell technique consists of a reformulation of the Floquet-Bloch partial differential problem, in which the phase shift of the boundary conditions related to wave propagation is integrated into the derivation operator. Consequently, the periodicity is included in the overall behavior of the structure while the continuity conditions are imposed at the edges of the unit cell. Its major advantage is that it allows to implement any frequency dependence and damping in the problem; this is essential, if one needs to compute the dispersion curves of a porous material modelled as an equivalent fluid. In detail, it allows the description of the propagation of all existing waves from the description of the unit cell through the resolution of a quadratic eigenvalue problem. This is done through the $k(\omega)$ method, that allows to compute dispersion curves for frequency-dependent problems, instead of using the $\omega(k)$ one that leads to non-linear eigenvalue problems.

A validation of the implementation of this model in order to handle porous materials with periodic inclusions, together with a detailed explication of the meaning and the behavior of band gaps, can be found in literature [2].

Dispersion curves and acoustical characteristics for different numerical test cases are shown. In particular, they are obtained for a 3D melamine unit cell, with and without inclusion. The behavior of this porous

material is described by JCA model in the following pages, but one can identically use any other equivalent fluid model.

The second part of this work concerns the investigation of the link between the dispersion curves and the acoustic properties of the material. In particular it's demonstrated that, starting from the wave numbers obtained as an output from the quadratic eigenvalue problem, it's possible to compute an equivalent transmission loss curve that, if compared to those obtained using classical methods, shows a very good agreement. Deriving the equivalent acoustic properties of the unit cell from its dispersion characteristics, indeed, could be a very efficient approach for designing sound packages with a simple a preliminary eigenvalue analysis.

All the results shown are related to a 3D melamine unit cell constituted by a cube with side equal to 2 [cm] (homogeneous case) and with a 0.5 [cm] radius cylindrical rigid inclusion (case with inclusion). The analyses are carried out in the frequency range 0 – 17000 [Hz]; this range of frequencies is interesting for acoustic applications and assures that the wavelength is much larger than the pore size, which is a necessary condition in order to use equivalent fluid models. Dispersion diagrams are computed along the direction that corresponds to $\phi = 0°$ and $\theta = 0°$ in the first Brillouin zone.

2 Shift cell operator technique

Considering a porous layer as an equivalent fluid [3], the starting equation for developing the associated shift cell formulation is

$$(\nabla + j\boldsymbol{k})^T \left(\frac{1}{\rho}(\nabla + j\boldsymbol{k})\boldsymbol{p}\right) = -\frac{\omega^2}{K}\boldsymbol{p}, \tag{1}$$

with $\rho = \rho(material, \omega)$ and $K = K(material, \omega)$.

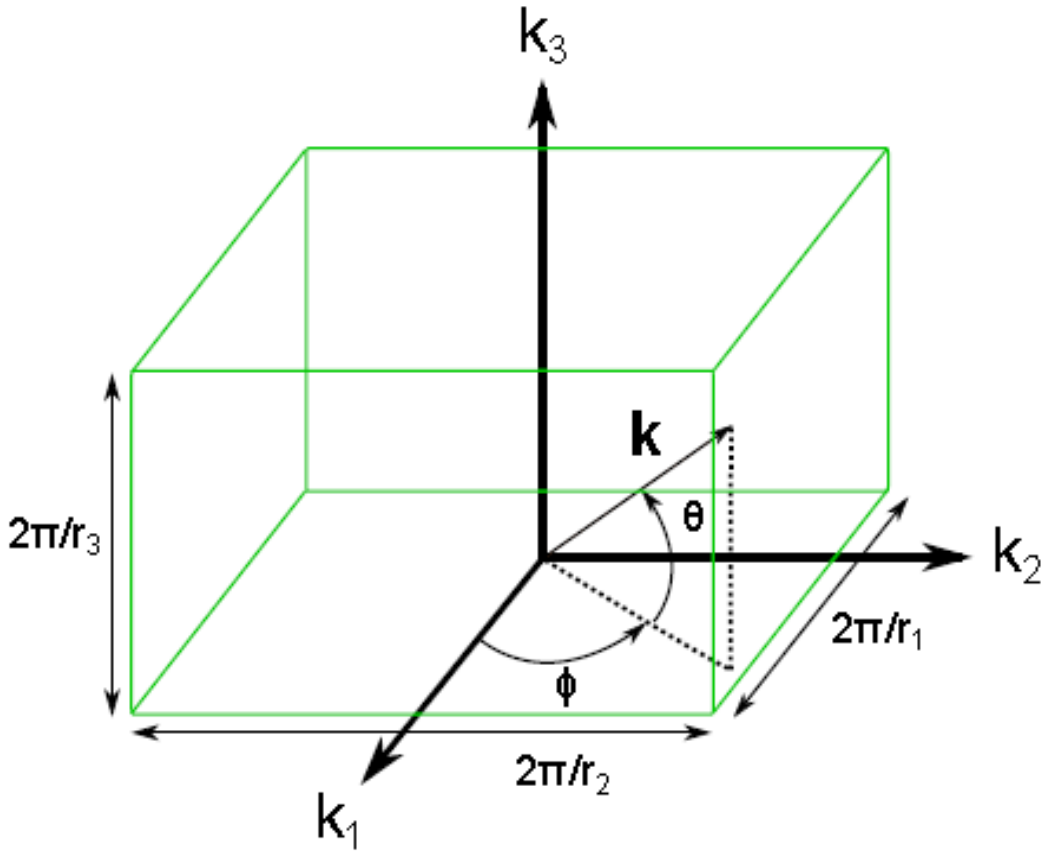

Figure 1: Reciprocal lattice vector in a 3D unitary cell [4].

By further developing the latter equation and considering $\boldsymbol{p} = pe^{j\boldsymbol{kx}}$ where $\boldsymbol{k}$, for a 3D application (Figure 1), is

$$\boldsymbol{k} = k\boldsymbol{\phi}, \boldsymbol{\phi} = \begin{pmatrix} cos\theta cos\phi \\ cos\theta sin\phi \\ sin\theta \end{pmatrix}, \tag{2}$$

one can obtain

$$\nabla^T \frac{\nabla(pe^{j\boldsymbol{kx}})}{\rho} + j\boldsymbol{k}^T \left(2\frac{\nabla(pe^{j\boldsymbol{kx}})}{\rho} + pe^{j\boldsymbol{kx}}\nabla\frac{1}{\rho}\right) - \boldsymbol{k}^T\boldsymbol{k}\frac{pe^{j\boldsymbol{kx}}}{\rho} + \frac{\omega^2}{K}pe^{j\boldsymbol{kx}} = 0. \tag{3}$$

2.1 Weak formulation

The weak formulation is calculated from the following equation, where $\tilde{p}$ is a weighting test function:

$$\int_\Omega \tilde{p}e^{-j\boldsymbol{k}^T\boldsymbol{x}}\left(\nabla^T \frac{\nabla(pe^{j\boldsymbol{kx}})}{\rho} + j\boldsymbol{k}^T \left(2\frac{\nabla(pe^{j\boldsymbol{kx}})}{\rho} + pe^{j\boldsymbol{kx}}\nabla\frac{1}{\rho}\right) - \boldsymbol{k}^T\boldsymbol{k}\frac{pe^{j\boldsymbol{kx}}}{\rho} + \frac{\omega^2}{K}pe^{j\boldsymbol{kx}}\right)d\Omega = 0 \tag{4}$$

$$\int_\Omega \left(\frac{1}{\rho}\nabla^T\tilde{p}\nabla p - j\boldsymbol{k}^T\frac{2}{\rho}(\tilde{p}\nabla p - \nabla\tilde{p}p) + \boldsymbol{k}^T\boldsymbol{k}\frac{4}{\rho}\tilde{p}p - \omega^2\frac{1}{K}\tilde{p}p\right)d\Omega = 0 \tag{5}$$

Considering that $\boldsymbol{\varphi}$ is the eigenvector, the equation can be written in its matrix form

$$(\boldsymbol{K} + jk\boldsymbol{L} + k^2\boldsymbol{H} - \omega^2\boldsymbol{M})\boldsymbol{\varphi} = 0 \tag{6}$$

with the following matrices:

- $\boldsymbol{K} \rightarrow \int_\Omega \frac{1}{\rho}\nabla\tilde{p}\nabla p\, d\Omega$;
- $\boldsymbol{L} \rightarrow \int_\Omega \frac{2}{\rho}(\nabla\tilde{p}p - \tilde{p}\nabla p)\, d\Omega$;
- $\boldsymbol{H} \rightarrow \int_\Omega \frac{4}{\rho}\tilde{p}p\, d\Omega$;
- $\boldsymbol{M} \rightarrow \int_\Omega \frac{1}{K}\tilde{p}p\, d\Omega$.

2.2 Right and left eigenvalue problems

The latter formulation leads to the following right eigenvalue problem:

$$\left[(\boldsymbol{K} - \omega^2\boldsymbol{M}) + \lambda_i\boldsymbol{L} - \lambda_i^2\boldsymbol{H}\right]\boldsymbol{\varphi}_i^r = 0 \tag{7}$$

where $\lambda_i = jk_i$ is the i-th eigenvalue, φ_i^r denotes the right eigenvector associated to λ_i, $\boldsymbol{M}$ and $\boldsymbol{K}$ are respectively the standard symmetric definite mass and symmetric semi-definite stiffness matrices, $\boldsymbol{L}$ is a skew-symmetric matrix and $\boldsymbol{H}$ is a symmetric semi-definite positive matrix. In this formulation, all matrices are frequency dependent.

For frequency-dependent systems, the estimation of the group velocity is not trivial. The equation (7) can be rewritten as

$$\boldsymbol{A}_1(\omega)\boldsymbol{\psi}_i^r = \lambda_i\boldsymbol{A}_2(\omega)\boldsymbol{\psi}_i^r \tag{8}$$

with

- $\boldsymbol{A}_1(\omega) = \begin{pmatrix} 0 & \boldsymbol{I_d} \\ \boldsymbol{K} - \omega^2\boldsymbol{M} & \boldsymbol{L} \end{pmatrix}$;
- $\boldsymbol{A}_2(\omega) = \begin{pmatrix} \boldsymbol{I_d} & 0 \\ 0 & \boldsymbol{H} \end{pmatrix}$;
- $\boldsymbol{\psi}_i^r = \begin{pmatrix} \boldsymbol{\varphi}_i^r \\ \lambda_i\boldsymbol{\varphi}_i^r \end{pmatrix}$.

where $\boldsymbol{I_d}$ is the identity matrix.

Conversely, a left-eigenvector for the same eigenvalue satisfies

$$\boldsymbol{\psi}_i^{l^T}\boldsymbol{A}_1(\omega) = \lambda_i \boldsymbol{\psi}_i^{l^T}\boldsymbol{A}_2(\omega), \text{ with } \boldsymbol{\psi}_i^l = \begin{pmatrix}\boldsymbol{A}\\ \boldsymbol{B}\end{pmatrix}. \tag{9}$$

$$\begin{cases} \boldsymbol{B} = \boldsymbol{\varphi}_{-i}^r = \boldsymbol{\varphi}_i^l \\ \boldsymbol{A}^T = \lambda_i \boldsymbol{\varphi}_{-i}^{r\,T}\boldsymbol{H} - \boldsymbol{\varphi}_{-i}^{r\,T}\boldsymbol{L} = \lambda_i \boldsymbol{\varphi}_i^{l^T}\boldsymbol{H} - \boldsymbol{\varphi}_i^{l^T}\boldsymbol{L} \end{cases} \tag{10}$$

In the resolution of the right eigenvalue problem, the i-th mode ($i \in N^+$) is defined by its $\lambda_i \geq 0$ and its eigenvector $\boldsymbol{\varphi}_i^r$. For each mode i, a mode $-i$ is associated with $\lambda_{-i} \leq 0$ such that $\lambda_{-i} = -\lambda_i$ and $\boldsymbol{\varphi}_{-i}^r = \boldsymbol{\varphi}_i^l$. by solving the right eigenvalue problem, the left solution is found too [4].

After some steps, one obtains the expression of the group slowness using $\lambda_i = jk_i$:

$$\frac{\partial k_i}{\partial \omega} = -j\frac{\boldsymbol{\varphi}_i^{l^T}\left[-2\omega\boldsymbol{M} + \frac{\partial \boldsymbol{K}}{\partial \omega} + \lambda_i \frac{\partial \boldsymbol{L}}{\partial \omega} - \lambda_i^2 \frac{\partial \boldsymbol{H}}{\partial \omega}\right]\boldsymbol{\varphi}_i^r}{\boldsymbol{\varphi}_i^{l^T}\left[-\boldsymbol{L} + 2\lambda_i \boldsymbol{H}\right]\boldsymbol{\varphi}_i^r} \tag{11}$$

The group velocity is the inverse of the group slowness [5]:

$$C_g = \frac{\partial \omega}{\partial k_i} = \frac{j\boldsymbol{\varphi}_i^{l^T}\left[-\boldsymbol{L} + 2\lambda_i \boldsymbol{H}\right]\boldsymbol{\varphi}_i^r}{\boldsymbol{\varphi}_i^{l^T}\left[-2\omega\boldsymbol{M} + \frac{\partial \boldsymbol{K}}{\partial \omega} + \lambda_i \frac{\partial \boldsymbol{L}}{\partial \omega} - \lambda_i^2 \frac{\partial \boldsymbol{H}}{\partial \omega}\right]\boldsymbol{\varphi}_i^r} \tag{12}$$

2.3 Classifying criteria to distinguish propagative and evanescent waves

Applying the shift cell operator technique to a sample modelled by an equivalent fluid, all the wave numbers are complex; consequently, there are not purely propagative solutions anymore. All waves are evanescent, with an evanescence rate that may be used to classify the branches in two categories: those that will be rapidly damped and those that will be slowly damped in space, with the latter that could be classified as propagative ones.

The distinction between the two is difficult and thus some classifying criteria are required:

1. the ratio between the real and the imaginary parts of every wavenumber → $C_1 = real(k)/imag(k)$;
2. the ratio between the real parts of the energy transport speed $v_E = I/E$ and the goup velocity C_g, where I is the flow of energy and $E = E_k + E_p = \int_\Omega \frac{1}{2}\left(\rho v^2 + \frac{p^2}{\rho c^2}\right) d\Omega$ is the total energy → $C_2 = real(v_E)/real(C_g)$.

Only the waves corresponding to $C_1 > \tau_1$ and $C_2 > \tau_2$ are considered as propagative ones. In practice, for the purpose of the following analysis, the thresholds τ are chosen such as $\tau_1 = 1$ and $\tau_2 = 0.7$. This is an arbitrary choice and these values are not meant to be considered as universal: for each different case, one may need to tune them [4]. In order to better appreciate the behavior of each branch in the frequency range of study in the following plots, dispersion and C_g curves are also colorized with a scale of colors that indicates the level of "propagativeness": the value 0 means that the wave at that specific frequency is totally spatially attenuated, while the value 1 represents a properly propagative behavior.

3 Calculation of group velocity and branch-tracking algorithm

In a dispersion diagram there is a set of points, forming branches, that one may wish to connect and follow according to the nature of each branch. Some solutions are proposed in literature, such as a MAC sorting criterion [6], but these methods require to store many data at every iteration. Instead, the group velocity constitutes a relevant indicator in order to follow the branches from a point of calculation to the next one [4]. The proposed technique consists in comparing $C_{g_i}(f)$ and $\boldsymbol{C_g}(f + \Delta f)$: from the group velocity

associated to a starting point, the routine compares the initial C_{g_i} with all the group velocities at the next frequency step and a minimization is made in order to identify the point at $f + \Delta f$ to which is associated the closest value of C_g. This point is defined as the new starting one and so on, step by step, the branch is identified.

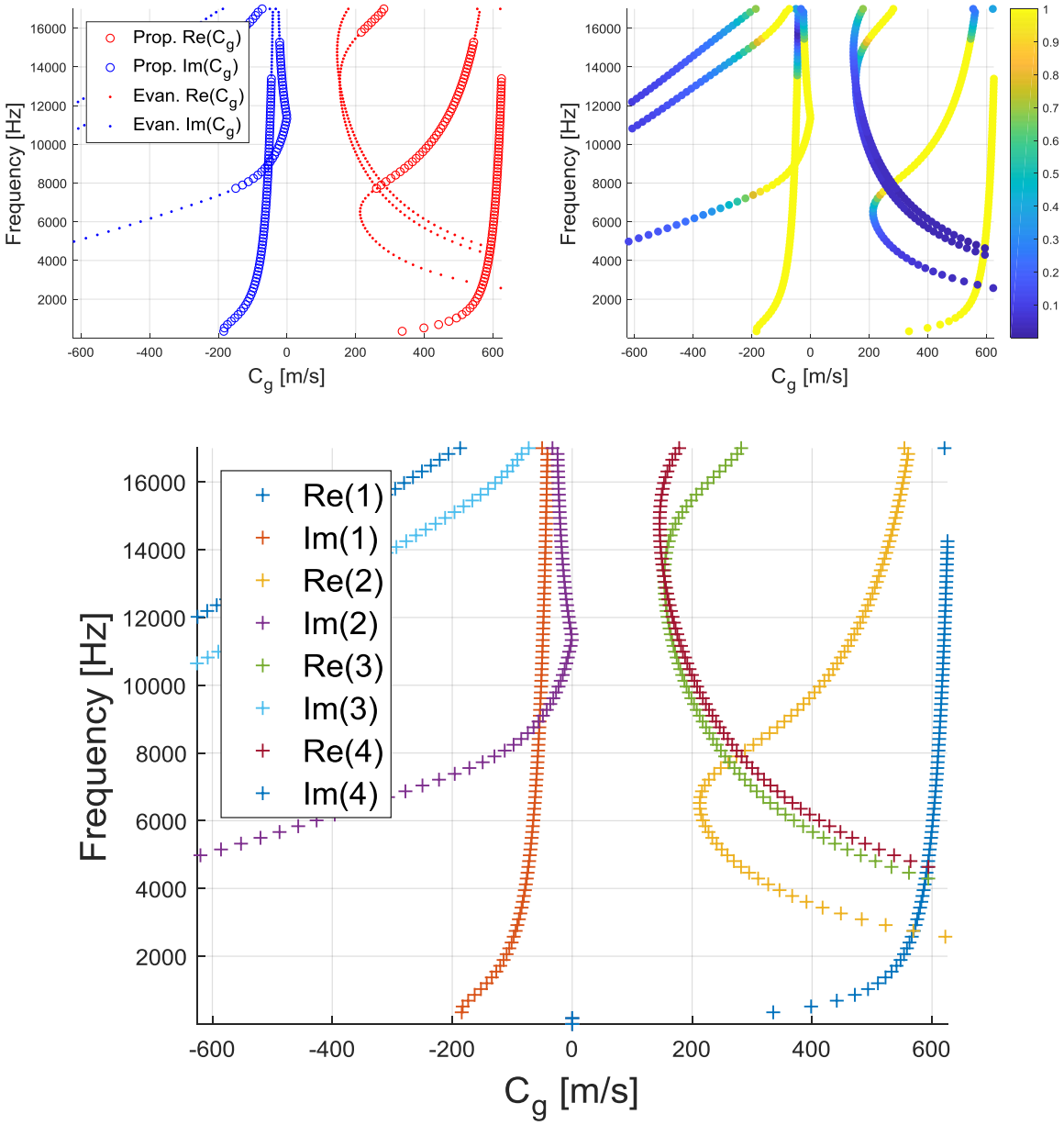

Figure 2: Evanescent and propagative (on the top) and branch-tracked (on the bottom) group velocity diagrams, for the case of a homogeneous unit cell.

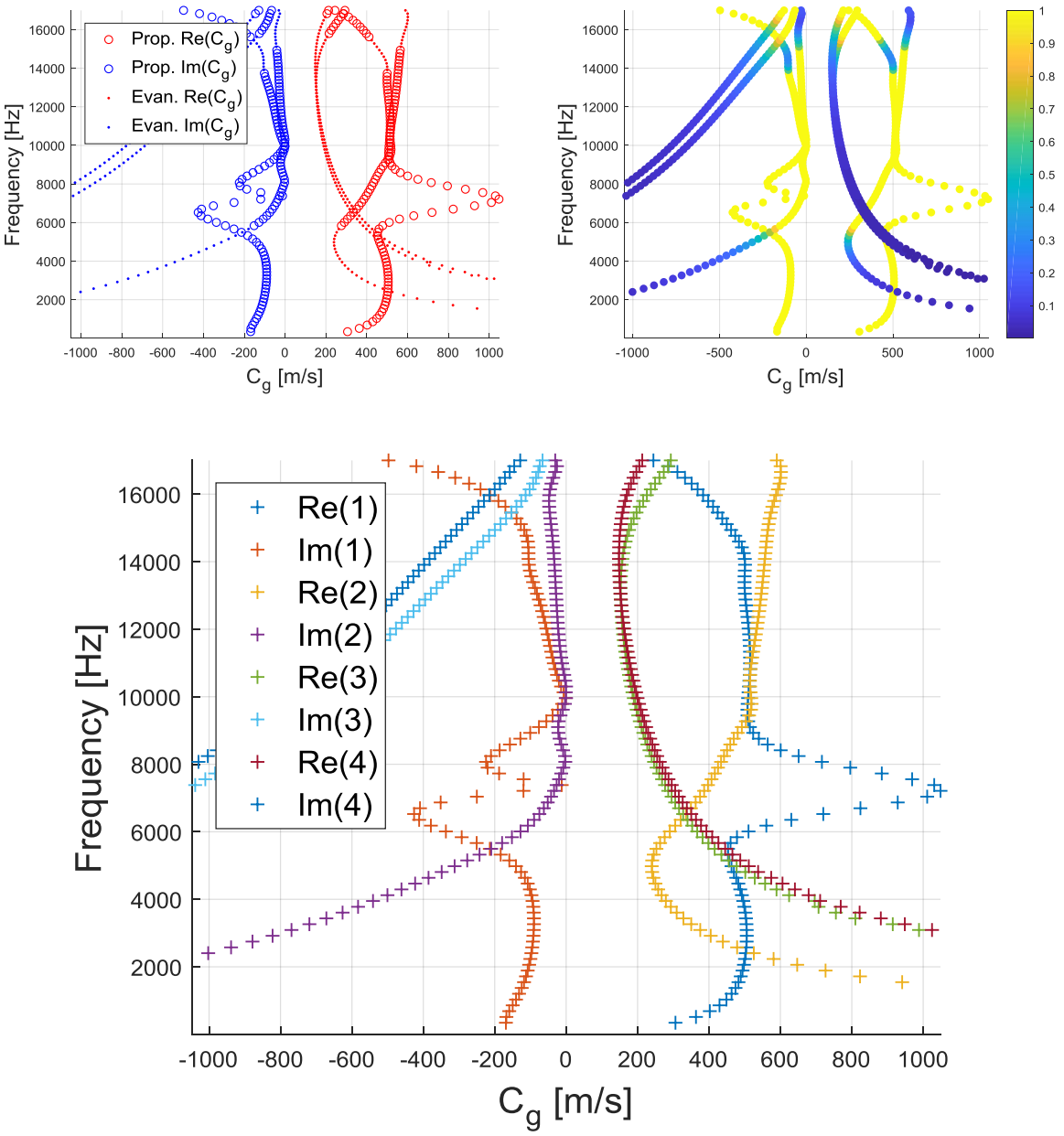

Figure 3: Evanescent and propagative (on the top) and branch-tracked (on the bottom) group velocity diagrams, for the case of an unit cell with an inclusion.

4 Dispersion curves

For each dispersion curve plot, three eigenvectors are reported in terms of acoustic pressure field (Figures 5 and 7). Only the real parts are shown, the imaginary parts being null. They are all extracted at the frequency of 8500 [Hz] (half of the range) and along the direction that corresponds to $\theta = \phi = 0°$ in the first Brillouin zone. Their branches are ordered as: at increasing frequencies, 1st is represented by the first real part that reaches the unitary value, 2nd is the second and so on. The fundamental acoustic parameters of the tested porous material have been experimentally determined in GAUS laboratory at University of Sherbrooke (Canada) and are: porosity $= 0.99$, tortuosity $= 1.02$, resistivity $= 8430 \left[\frac{Pa*s}{m^2}\right]$, viscous characteristic length $= 0.138\ [mm]$, thermal characteristic length $= 0.154\ [mm]$, density $= 5.73\ \left[\frac{kg}{m^3}\right]$.

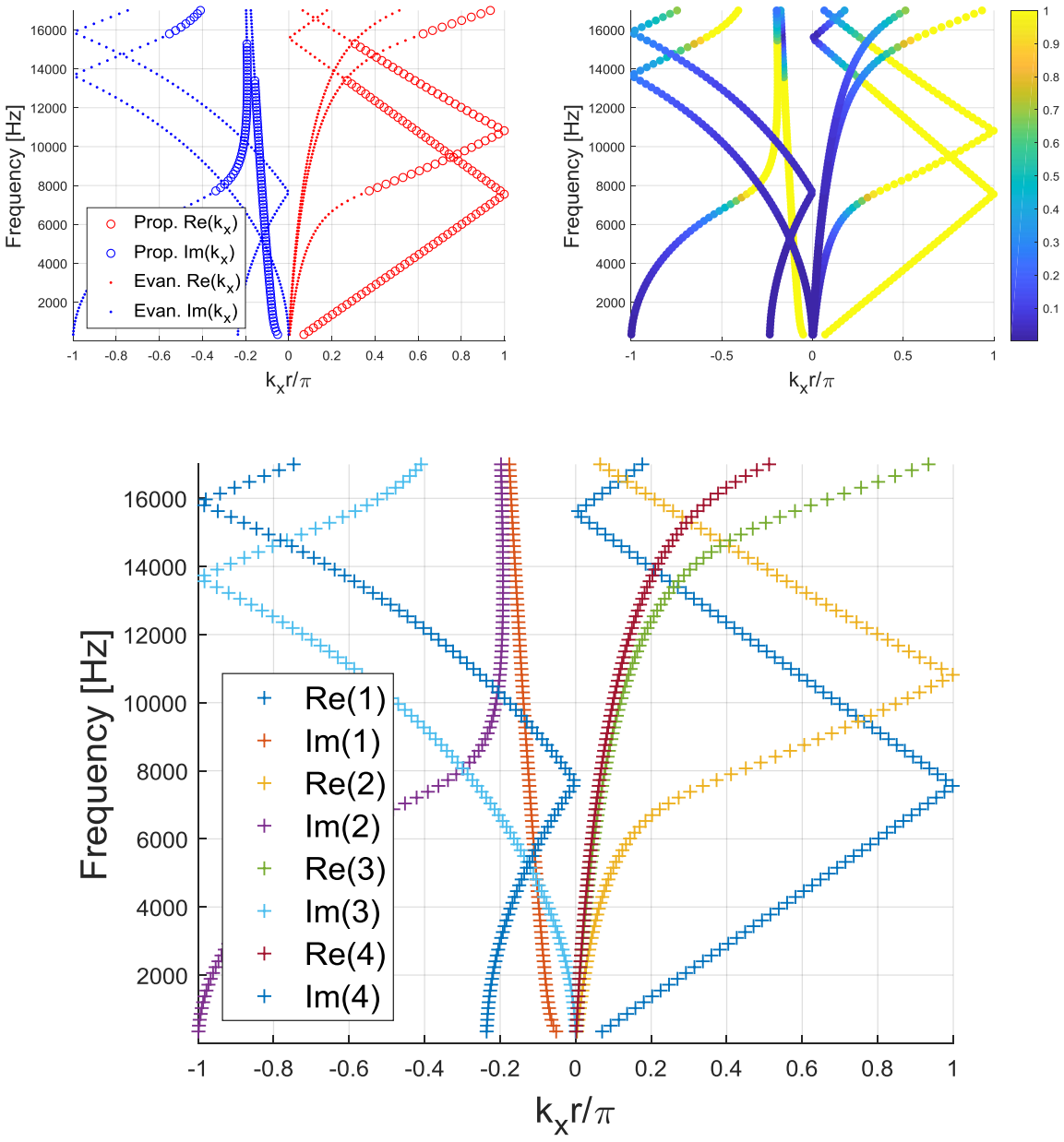

Figure 4: Evanescent and propagative (on the left) and branch-tracked (on the right) dispersion curves for a homogeneous melamine unit cell.

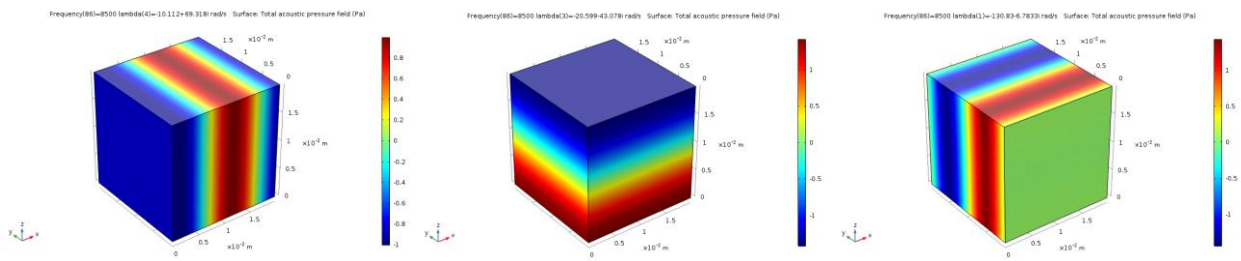

Figure 5: From left to right, real parts of the 1st, 2nd and 3rd branch eigenvectors for the homogeneous case.

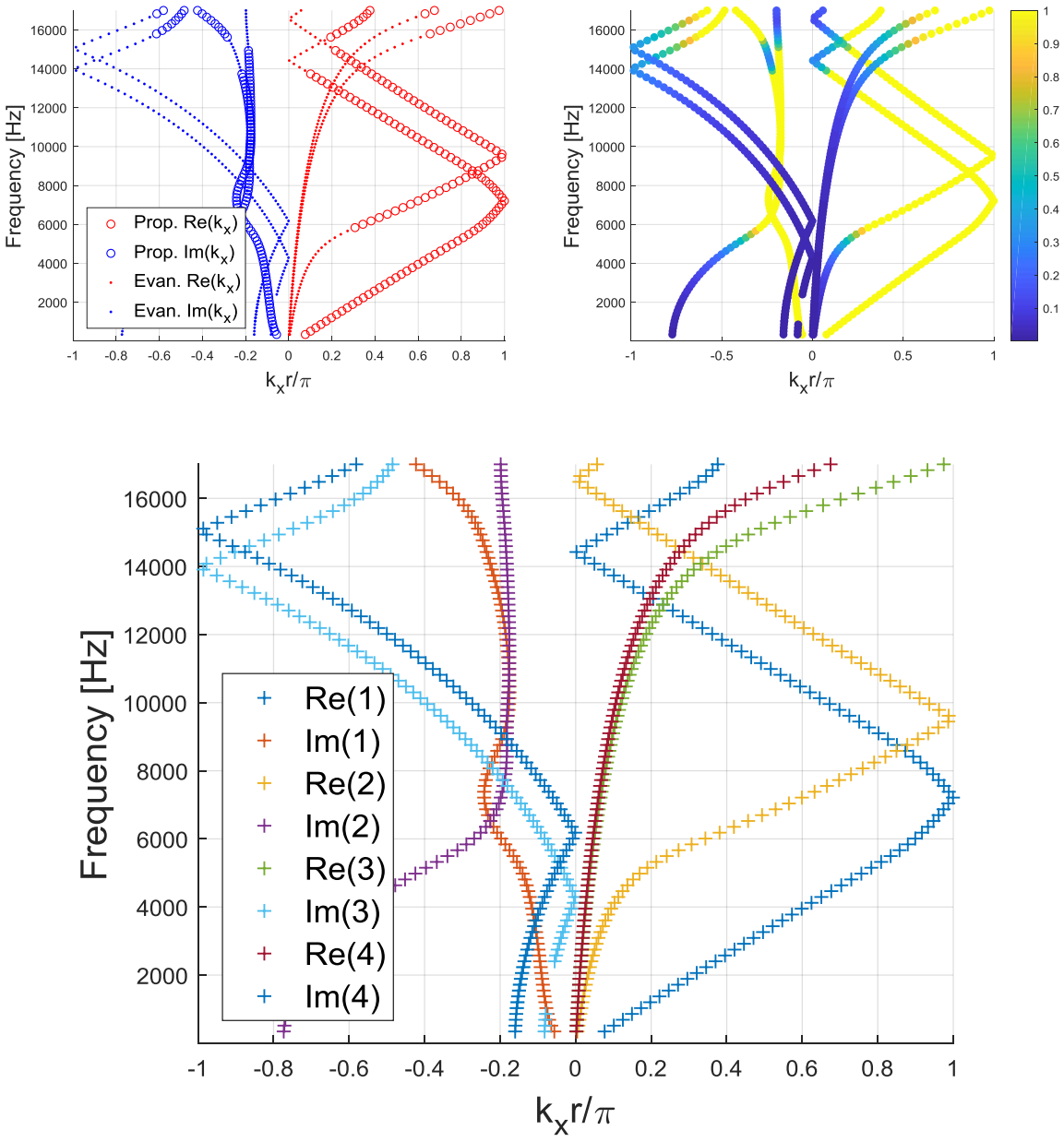

Figure 6: Evanescent and propagative (on the left) and branch-tracked (on the right) dispersion curves for a melamine unit cell with an inclusion.

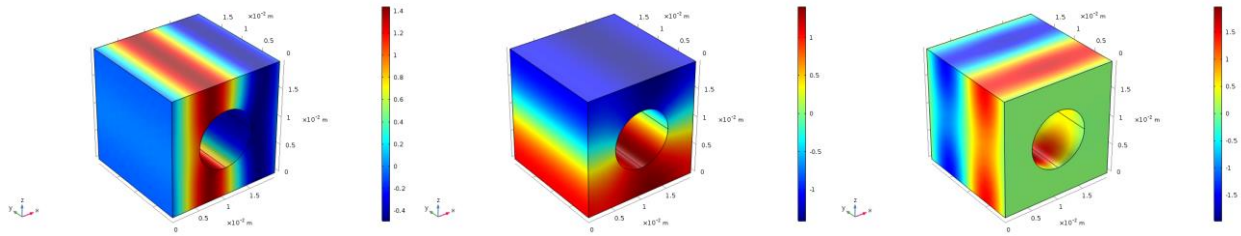

Figure 7: From left to right, real parts of the 1st, 2nd and 3rd branch eigenvectors for the case with an inclusion.

One may notice that there are some discontinuous curves: this is probably due to the fact that, as said, all waves are evanescent with different rates: a non-perfect tuning of the sorting criteria could lead to lines that disappears and reappears on the plots.

5 Transmission loss

While dispersion curves are computed for an infinite repetition of unit cells, transmission loss is calculated for a finite repetition of 5 unit cells, using the same domain and boundary conditions of the infinite periodic system. This, in a first approximation, allows to compare the dispersion relations and the acoustical characteristics of the equivalent finite medium. Indeed, a further increasing in the number of repeated cells would lead to a change in the mean value of absorption coefficient and transmission loss respectively below 2% and 20% respect to the usage of a repetition of 5 unit cells.

The transmission loss is numerically computed as

$$TL = 10\log_{10}\frac{\Pi_{incident}}{\Pi_{transmitted}} \tag{13}$$

where $\Pi_{incident}$ and $\Pi_{transmitted}$ represent the incident and transmitted power, respectively. For our plane wave configuration, the latter is compared, for homogeneous flat configurations, with the Transfer matrix method [7]:

$$TL = 10\log\left(\frac{1}{4}\left|T_{11} + \frac{T_{12}}{\rho_0 c_0} + \rho_0 c_0 T_{21} + T_{22}\right|^2\right), \tag{14}$$

$$\text{with } \begin{bmatrix} T_{11} & T_{12} \\ T_{21} & T_{22} \end{bmatrix} = \begin{bmatrix} \cos(kd) & j\sin(kd)\, Z_c \\ \frac{j\sin(kd)}{Z_c} & \cos(kd) \end{bmatrix} \tag{15}$$

For the inhomogeneous configuration, the validation is obtained using an implementation of the plane wave forced response of the periodic cell accounting for fluid loading [8].

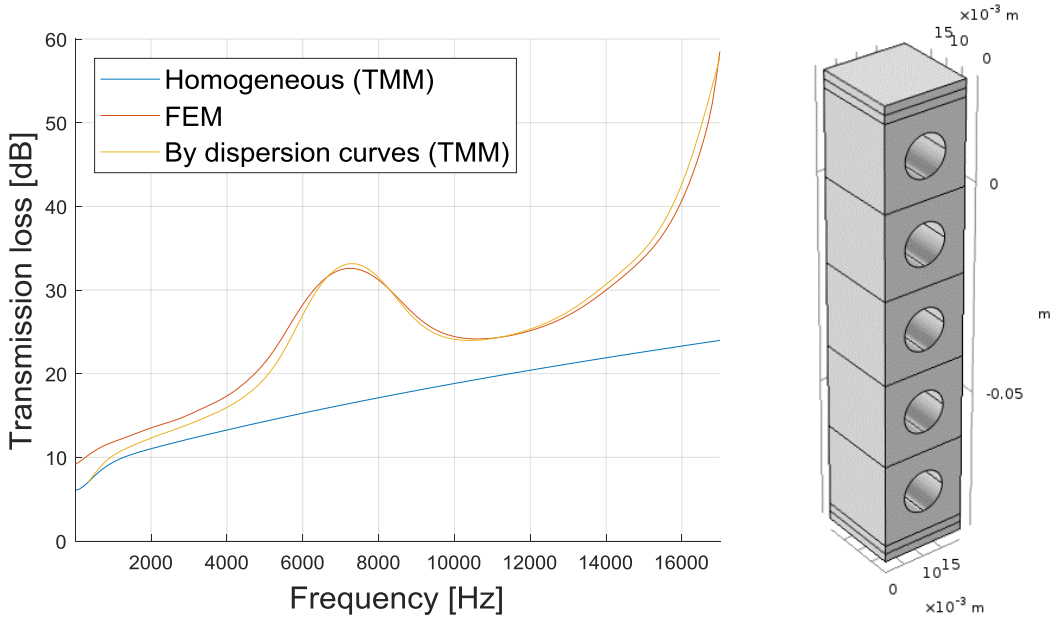

Figure 8: Transmission loss computed for a 3D repetition of 5 melamine unit cells.

Concerning the case with the inclusion, one can notice that an improvement of transmission loss properties, respect to the homogeneous case, is shown at all frequencies, in particular in correspondence of a peak at a frequency around 7 [kHz], in which it is equal to about 15 [dB], and at high frequencies. Note that, for the sake of comparison with the related dispersion curves, only their 1st branch is meaningful due to the fact that the correspondent mode is the only one that is actually excited during these transmission loss simulations. Indeed, the improvement peak exactly corresponds to the frequency range of the 1st branch of dispersion curves in which the wave is strongly spatially attenuated.

This is definitely encouraging, for the purpose of deriving more equivalent acoustic properties of the unit cell from its dispersion characteristics.

6 Conclusions

The shift cell technique has been presented, providing details on its numerical formulation. It has been necessary to introduce some classifying criteria and, consequently, the derivation of the group velocity expression. A branch-tracking criterion has been described, in order to clearly identify each branch in the dispersion diagram. Dispersion curves and transmission loss plots have then been computed for a JCA-modelled melamine unit cell. An equivalent transmission loss curve, obtained starting from the eigenvalues, has been compared to those obtained with classical methods, showing a very good agreement. Further developments of the work will include an estimation of the computational efficiency between the shift cell and the classical Floquet-Bloch approaches, as well as the implementation of the shift cell technique using Biot model.

Acknowledgements

This project has received funding from the European Union's Horizon 2020 research and innovation program under the Marie Skłodowska-Curie grant agreement No. 675441.

References

[1] D. Magliacano, M. Ouisse, A. Khelif, S. De Rosa, and F. Franco, "The shifted cell operator technique applied to equivalent fluids models for the computation of dispersion diagrams of periodic porous materials," in *SAPEM 2017 proceedings*, 2017.

[2] D. Magliacano *et al.*, "Validation of shift cell approach for the modelling of acoustic properties of porous materials embedding periodic inclusions," in *NOVEM 2018 proceedings*, 2018, pp. 1–11.

[3] O. Doutres, Y. Salissou, N. Atalla, and R. Panneton, "Evaluation of the acoustic and non-acoustic properties of sound absorbing materials using a three-microphone impedance tube," *Appl. Acoust.*, vol. 71, no. 6, pp. 506–509, 2010.

[4] K. Billon, "Composites periodiques fonctionnels pour l'absorption vibroacoustique large bande," *PhD thesis Univ. Fr.*, 2017.

[5] R. P. Moiseyenko and V. Laude, "Material loss influence on the complex band structure and group velocity in phononic crystals," *Phys. Rev. B - Condens. Matter Mater. Phys.*, vol. 83, no. 6, pp. 1–6, 2011.

[6] M. Collet, M. Ouisse, M. Ruzzene, and M. N. Ichchou, "Floquet-Bloch decomposition for the computation of dispersion of two-dimensional periodic, damped mechanical systems," *Int. J. Solids Struct.*, vol. 48, no. 20, pp. 2837–2848, 2011.

[7] J. F. Allard and N. Atalla, *Propagation of Sound in Porous Media: Modelling Sound Absorbing Materials*. 2009.

[8] N. Atalla, *NOVAFEM User's guide*. Sherbrooke (QC, Canada): Université de Sherbrooke, 2017.